Drag reduction by streamwise traveling wave-like Lorenz Force in channel flow

Hiroya Mamori & Koji Fukagata

Department of Mechanical Engineering, Keio University, JAPAN

E-mail: hiroyamamori@z5.keio.jp

Abstract. Skin-friction drag reduction effect of traveling wave-like wall-normal Lorenz force in a fully developed turbulent channel flow is investigated by means of direct numerical simulation. A sinusoidal profile of the wall-normal body force is assumed as the Lorenz force. While upstream traveling waves reduce the drag in the case of blowing/suction, standing waves reduce it in the case of present forcing. Visualization of vortical structure under the standing wave-like wall-normal Lorenz force reveals that the near-wall streamwise vortices, which increase the skin-friction drag, disappear and spanwise roller-like vortices are generated instead. Three component decomposition of the Reynolds shear stress indicates that the spanwise roller-like vortices contribute to the negative Reynolds shear stress in the region near the wall, similarly to the case of laminar flows. While the analogy between the wall-normal and streamwise forcings can be expected, the statistics are found to exhibit different behaviors due to the difference in the energy flow.

1. Introduction

The skin-friction significantly increases when the flow becomes turbulent. Therefore, turbulence control aiming at skin-friction drag reduction has extensively been investigated because it is expected to contribute the energy saving and less environmental impact (Kasagi, Suzuki, & Fukagata (2009)). The investigation has often been made in fully developed channel flows because the existence of two homogeneous directions simplify the analysis. The skin-friction coefficient of a fully developed channel flow can be divided into the laminar and turbulent contributions, as (Fukagata, Iwamoto, & Kasagi (2002), Bewley & Aamo (2004))

$$C_f = \frac{12}{\mathrm{Re_b}} + 12 \int_0^1 2(1-y)\left(-\overline{u'v'}\right) dy, \tag{1}$$

where C_f and $\mathrm{Re_b}$ denote the skin-friction coefficient and the bulk Reynolds number, respectively, and the walls are located at $y = 0$ and 2 (made dimensionless by the channel half-width). The single prime denotes the fluctuation. Because the turbulent contribution, i.e., the second term of the RHS of this equation, is the integration of the y-weighted Reynolds shear stress ($-\overline{u'v'}$, hereafter referred to as RSS), control schemes for drag reduction should be designed to decrease the RSS in the region near the wall. Equation (1) implies that a sublaminar drag, i.e., the drag is lower than that of the laminar flow, is also possible when the negative RSS is obtained in the region near the wall (the RSS is ordinally positive).

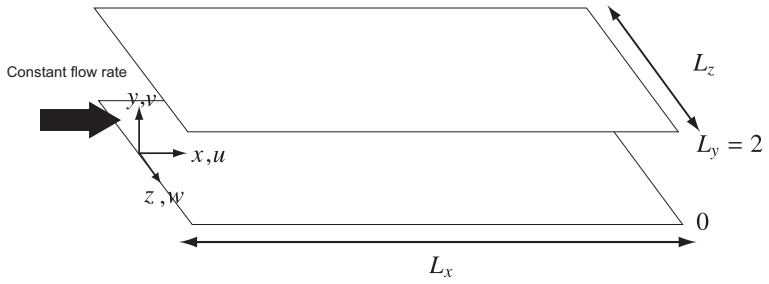

Figure 1. Two-dimensional plane channel flow under constant flow rate.

Based on this implication, Min, Kang, Speyer, & Kim (2006) proposed a streamwise traveling wave-like blowing/suction. Their control succeeded to sustain a sublaminar drag both in laminar and turbulent flows: the negative RSS was induced in the region near the wall when the wave travels to the upstream direction. Mamori, Fukagata, & Hœpffner (2010) reproduced Min *et al* 's laminar flow results and revealed by means of a linear analysis and a detailed phase analysis the mechanism to induce this negative RSS. The viscosity induces the phase lead of the streamwise velocity fluctuation from the wall-normal velocity fluctuation and the non-quadrature between them induced thereby makes the RSS negative.

Min *et al* reports that such negative RSS also appears in a turbulent flow in contrast to the ordinary situation, i.e., positive RSS.

The objective of this paper is to clarify by means of direct numerical simulation the mechanism of negative RSS production in a fully developed channel flow. Instead of traveling wave-like blowing/suction (Min, Kang, Speyer, & Kim (2006)), traveling wave-like wall-normal or streamwise Lorenz force is employed, which may be realized by electro-magneto-hydrodynamic (EMHD) actuators. Three component decomposition is adopted in order to investigate the contribution from the phase-averaged component. The contribution from phase-averaged component is compared with the phase relationship in the laminar flow obtained by a linear analysis. The analogy between the wall-normal and streamwise forcings are also discussed.

2. Direct numerical simulation and Control parameters

We consider a fully developed channel flow as shown in Fig. 1. Here, the streamwise, wall-normal, and spanwise coordinates and velocities are denoted as (x, y, z) and (u, v, w) (or (x_1, x_2, x_3) and (u_1, u_2, u_3)), respectively. The coordinates and the velocities are made dimensionless by using the channel half-width δ^* and twice the bulk velocity $2u_b^*$, where the asterisk denotes the dimensional quantity.

With this nondimensionalization, the governing equations for this channel flow read

$$\frac{\partial u_i}{\partial x_i} = 0, \tag{2}$$

$$\frac{\partial u_i}{\partial t} + \frac{\partial u_j u_i}{\partial x_j} = -\frac{\partial p}{\partial x_i} + \frac{1}{\mathrm{Re}_b}\frac{\partial^2 u_i}{\partial x_j \partial x_j} + F_i. \tag{3}$$

The no-slip for the velocities on the wall and the periodic conditions for the homogeneous directions are employed. The direct numerical simulation is performed under a constant mass flow rate. The bulk Reynolds number is set at $\mathrm{Re}_b = 5600$, which corresponds to $\mathrm{Re}_\tau \approx 177$ based on the friction velocity of the uncontrolled flow. The computational code is based on the DNS code of Fukagata, Kasagi, & Koumoutsakos (2006). All the simulations are started from the

velocity field of an uncontrolled fully developed channel flow. The size of compuational domain and the number of grid points are $L_x \times L_y \times L_z = 4\pi \times 2 \times 3.5$ and $N_x \times N_y \times N_z = 256 \times 96 \times 128$, respectively.

The body force term, F_i in Eq. (3), is a control input. The idealized Lorenz force is substituted into this F_i. It has a sinusoidal form in the streamwise direction and is damped in the wall-normal direction (Berger, Kim, Lee, & Lim (2000)). The traveling wave-like wall-normal Lorenz force reads

$$\begin{cases} F_x &= F_z = 0, \\ F_y &= I \exp\left(-\dfrac{y^+}{\Delta^+}\right) \cos\left(k\left(x - ct\right)\right), \end{cases} \tag{4}$$

for the lower half of the channel. Here, I and Δ^+ are the amplitude and the penetration length of the Lorentz force, respectively. The superscript of $+$ denotes the wall unit. The wavenumber and the wavespeed are denoted as k and c, respectively. A similar body force with the opposite sign is applied in the upper half of channel. Similarly, the streamwise Lorenz Force is expressed as

$$\begin{cases} F_x &= I \exp\left(-\dfrac{y^+}{\Delta^+}\right) \cos\left(k\left(x - ct\right)\right), \\ F_y &= F_z = 0. \end{cases} \tag{5}$$

3. Wall-normal Lorenz force

Figure 2(a) shows the drag reduction rate, defined as $R = \frac{C_{f_0} - C_f}{C_{f_0}}$, as a function of the wavespeed for different wavenumbers. The subscript of "0" denotes the uncontrolled value. The penetration length and amplitude are fixed at $\Delta^+ = 10$ and $I = 1.0$. The drag reduction rate is found to be positive (i.e., the drag reduction) at $c = 0$ and it is almost zero or negative when the wave travels. Namely, only the standing wave decreases the skin-friction drag in contrast to the case of blowing/suction (Min, Kang, Speyer, & Kim (2006)). The efficiency, however, is found to be poor or negative for considered parameters (not shown) because the body force requires larger amount of actuation power than the blowing/suction does. Figure 2(b) shows the drag reduction rate by the standing wave as a function of wavenumber for two different penetration lengths. The maximum drag reduction is obtained at $k = 8$ for both penetration lengths. In the following, a parameter set of ($I = 1$, $c = 0$, $k = 8$ and $\Delta^+ = 10$) is chosen as a reference case.

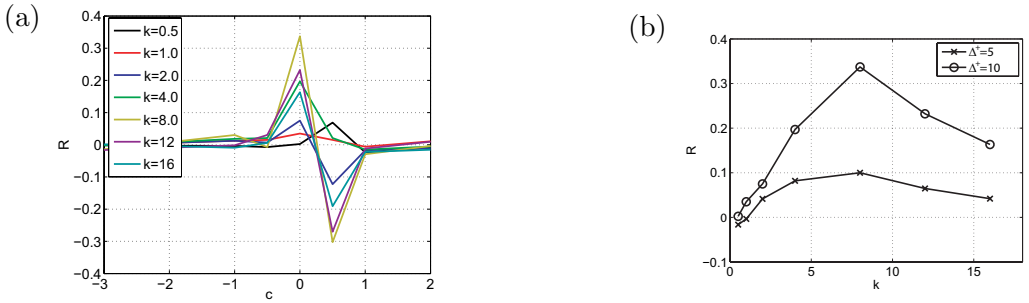

Figure 2. (a) Drag reduction rate as a function of wavespeed for different wavenumber ($I = 1.0$ and $\Delta^+ = 10$). (b) Drag reduction rate by the standing wave as a function of wavenumber for different penetration lengths. ($I = 1.0$)

Figure 3 visualizes the vortex cores in the lower half of the channel, which are identified by the isosurfaces of the second invariant of the velocity deformation tensor. Quasi-streamwise vorticies are pronounced in the uncontrolled flow as shown in Fig. 3. Because they exchange the

momentum between the near-wall and the far-wall regions, the positive RSS is produced and the skin-friction drag increases. Figure 3 shows the near-wall flow structure under the reference case with 35% drag reduction. While the near-wall vortex is found to disappear, the spanwise roller-like vortex is observed. Such spanwise roller-like vortex is known to induce the slip velocity and lead to drag reduction (Koumoutsakos (1999), Bewley (2001), Fukagata, Kasagi, & Sugiyama (2005)).

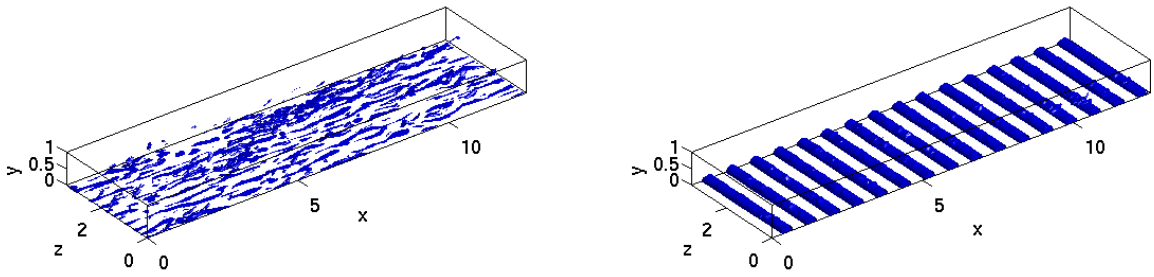

Figure 3. Visualization of vortexes ($Q^+ = -0.05$) in the lower half of the channel:left, uncontrolled flow;right, controlled by wall-normal Lorentz force (reference case: $I = 1.0$, $\Delta^+ = 5$, $k = 8.0$, and $c = 0.0$).

Three component decomposition (Hussain & Reynolds (1970)) is employed in order to distinguish the contributions from the spanwise roller-like vortices and the quasi-streamwise vortices, i.e.,

$$f = \overline{f} + \widetilde{f} + f'', \tag{6}$$

where the bar, the tilde, and the double primes denote the mean, phase, and random components. respectively. The sum of $\widetilde{f}$ and f'' is equivalent to f'. The averaging procedures are expressed as

$$\langle f \rangle (\phi_x, y) = \frac{1}{L_z T} \int_0^{L_z} \int_0^T \left(\lim_{N\to\infty} \frac{1}{N} \sum_{n=0}^{N} f(\phi_x + 2\pi n, y, z, t) \right) dt dz, \tag{7}$$

$$\overline{f}(y) = \frac{1}{2\pi} \int_0^{2\pi} \langle f \rangle \, d\phi_x, \tag{8}$$

$$\widetilde{f}(\phi_x, y) = \langle f \rangle - \overline{f}, \tag{9}$$

where ϕ_x is the coordinate of the wave (i.e., phase) in the streamwise direction, defined in $0 < \phi_x < 2\pi$.

According to abovementioned decomposition, the RSS $\left(-\overline{u'v'}\right)$ can be decomposed as

$$-\overline{u'v'} = -\overline{\widetilde{u}\widetilde{v}} - \overline{u''v''}. \tag{10}$$

where the first and second terms at the RHS are labeled as "phase-RSS" and "random-RSS", respectively. By substituting Eq. (10) into Eq. (1), the skin-friction coefficient can be rewritten as (Yakeno, Hasegawa, & Kasagi (2010))

$$C_f = \frac{12}{\mathrm{Re}_b} + 12 \int_0^1 2\,(1-y) \left(-\overline{\widetilde{u}\widetilde{v}}\right) dy + 12 \int_0^1 2\,(1-y) \left(-\overline{u''v''}\right) dy. \tag{11}$$

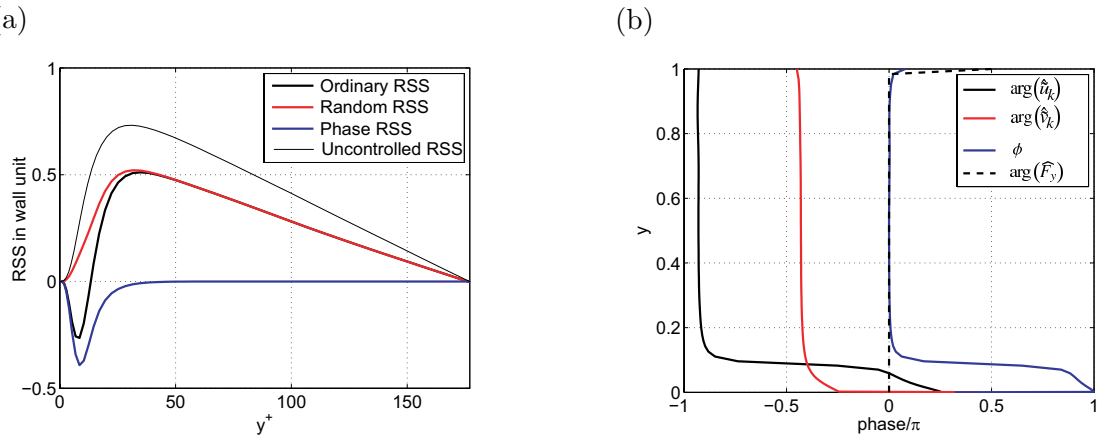

Figure 4. (a) Reynolds shear stress; (b) phase of the Fourier coefficients of velocities and body force.

Namely, the turbulent contribution by the RSS can be divided into the contributions from the phase-RSS and the random-RSS.

Figure 4(a) shows the profiles of these RSSs in the reference case. The RSS is found to be negative in the region near the wall due to the negative phase-RSS at $0 < y^+ < 40$. The random-RSS is found to decrease but kept positive.

According to the phase analysis by Mamori, Fukagata, & Hœpffner (2010), the RSS in a laminar flow is generated by the non-quadrature between the streamwise and wall-normal velocities fluctuations. The Fourier transform is defined as

$$f = \sum_{k'=0}^{N} \widehat{f}_{k'} e^{-ik'x} \tag{12}$$

where the hat denotes the Fourier coefficient. The phase difference between the Fourier coefficients of the streamwise and wall-normal velocities is defined as

$$\phi = \arg \widehat{\widetilde{u}}_k - \arg \widehat{\widetilde{v}}_k + \frac{\pi}{2} \tag{13}$$

where the wavenumber of the Fourier coefficients are chosen at $k' = k$. Figure 4(b) shows the phase relationship among the phase averaged velocities and the phase difference. The non-quadrature (i.e., $\phi \neq 0$ or $\pi/2$) appears at $0 < y < 0.1$, which corresponds to the layer of negative phase-RSS. This non-quadrature is due to the phase reversal of $\tilde{u}$ in the region near the wall.

Figure 5(a) shows the distribution of wall-normal Lorenz Force together with the phase-averaged velocity vector in the region near the wall. Spanwise roller-like vortices appear in the region where the Lorenz force is positive, while the flow is expanded in the negative body force region. Figure 5(b) shows the distribution of the product of the phase velocities, $-\tilde{u}\tilde{v}$. The negative and positive regions are found around and inside the spanwise roller-like vortices, which contributes to $-\overline{\tilde{u}\tilde{v}} < 0$ as shown in Fig. 4(a).

Figure 6 explains the mechanism how the negative phase-RSS is produced around the spanwise roller-like vortex. The positive and negative $-\tilde{u}\tilde{v}$ are generated inside this vortex due to the rotation of the vortex, where $\tilde{u} < 0$. Above this spanwise roller-like vortex, the fluid is accelerated because this vortex induces the slip velocity on the surface of the vortex and the bulk velocity is kept constant at any streamwise positions. Therefore, the fluid particle, labeled as "Fluid 1" , brings $\tilde{u} > 0$ and travels into the region near the wall due to the downward rush

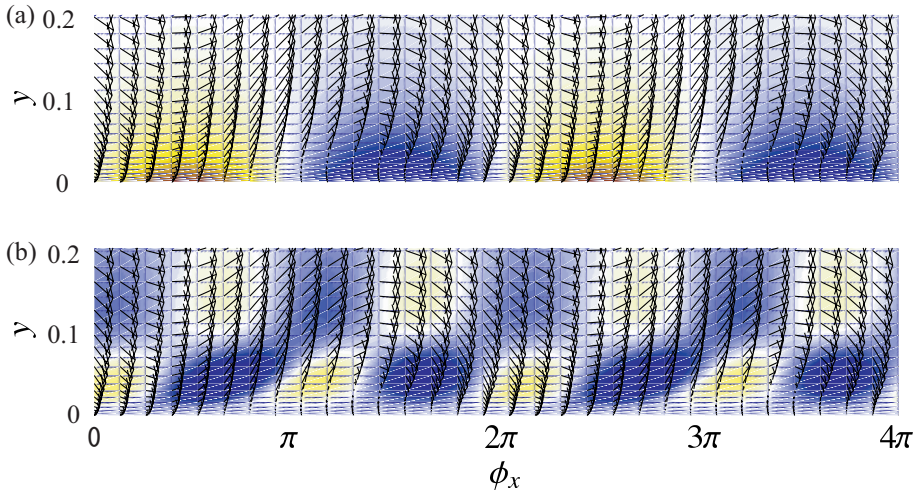

Figure 5. (a) Body force (the standing wave-like wall-normal Lorenz force); (b) product of the phase velocities, $-\widetilde{u}\widetilde{v}$, with velocity vector in the region near the wall of the reference case. The domain for the streamwise direction is extended for twice. The color of red and blue indicates the positive and negative value, respectively.

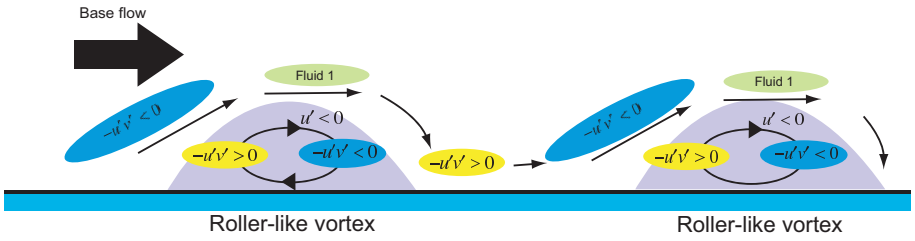

Figure 6. Mechanism how the phase RSS is generated around and inside the spanwise roller-like vortex.

($\tilde{v} < 0$) of the roller-like vortex, where $-\tilde{u}\tilde{v} > 0$ is generated. After the convection of "Fluid 1" to the downstream direction, it is pushed up by the upward rush induced by the rotation of the spanwise roller-like vortex; thus, $-\tilde{u}\tilde{v} < 0$ is generated. Because the mean velocity is imposed, more $-\tilde{u}\tilde{v} < 0$ is generated than $-\tilde{u}\tilde{v} > 0$.

3.1. Comparison with Linear analysis

In the fully developed turbulent channel flow, the negative phase-RSS is generated by the spanwise roller-like vortex induced by the forcing in the region near the wall. Here, the phase-averaged velocity is compared with the laminar flow case of the same input parameters. The controlled laminar velociy field is obtained by using the linear analysis (Mamori, Fukagata, & Hœpffner (2010)).

The governing equations are two-dimensional and linearized: $u = \overline{u} + \widetilde{u}$, $v = \widetilde{v}$, and $p = \overline{p} + \widetilde{p}$ are substituted into the Eqs. (2) and (3) and the high-order terms of phase component are

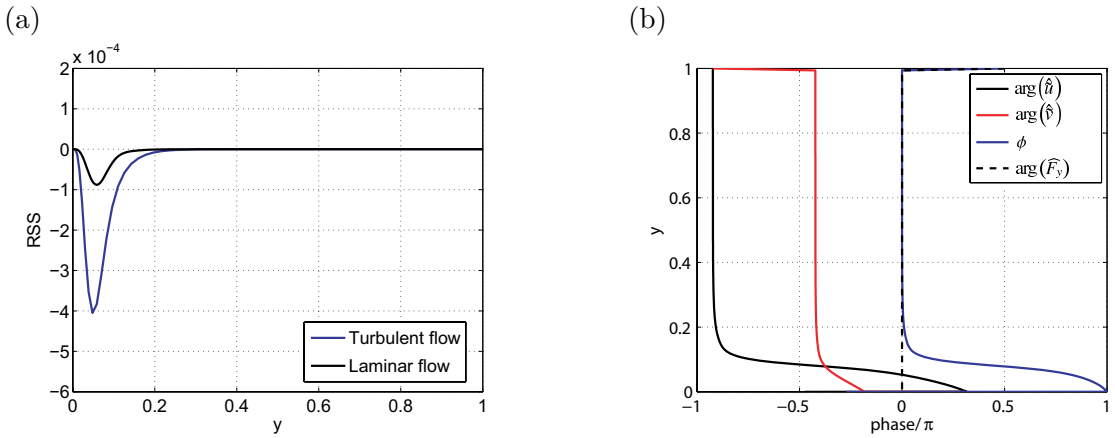

Figure 7. (a) Comparison of Reynolds shear stress profiles in the turbulent and laminar flows. (b) Phase profiles of the Fourier coefficient of the velocities and the body force in the laminar flow.

neglected, i.e.,

$$\frac{\partial \widetilde{u}}{\partial x} + \frac{\partial \widetilde{v}}{\partial y} = 0, \tag{14}$$

$$\overline{u}\frac{\partial \widetilde{u}}{\partial x} + \widetilde{v}\frac{\partial \overline{u}}{\partial y} = -\frac{\partial \widetilde{p}}{\partial x} + \frac{1}{\mathrm{Re}_b}\frac{\partial^2 \widetilde{u}}{\partial x_k \partial x_k}, \tag{15}$$

$$\overline{u}\frac{\partial \widetilde{v}}{\partial x} = -\frac{\partial \widetilde{p}}{\partial y} + \frac{1}{\mathrm{Re}_b}\frac{\partial^2 \widetilde{v}}{\partial x_k \partial x_k} + F_y. \tag{16}$$

Here, the flow is steady because the control input is steady. Since this case is not a turbulent flow, the laminar Poiseuille flow profile is employed for the base flow under the same Reynolds number, $\mathrm{Re}_b = 5600$. These equations are solved by using the Fourier transform for the streamwise direction and the Chebyshev collocation method for the wall-normal direction. As a control input, the same form of the wall-normal Lorenz force is added as the body force term of Eq. (16). The control parameters are set the same as those of the reference case of the turbulent flow.

Figure 7(a) shows the comparison between the phase-RSSs, $-\widetilde{u}\widetilde{v}$, of the laminar and turbulent flows. In both cases, negative RSS is obtained in the region near the wall, while the negative peak in the turbulent flow is lager than that in the laminar flow. Figure 7(b) shows the phase profile of the Fourier coefficient, which is identical to that of the turbulent flow. Figure 8 shows that the distribution of the body force and the product of $\widetilde{u}$ and $\widetilde{v}$ (with the velocity vector) are also similar to the results of the turbulent flow. Therefore, it can be concluded that the spanwise roller-like vortex is well described by the linearized Navier-stokes equation.

4. Streamwise Lorenz force

Figure 9 shows the drag reduction rate as a function of the wavenumber for $\Delta^+ = 5$ and 10 controlled by the standing wave-like streamwise Lorenz force defined in Eq. (5). The maximum drag reduction rate is obtained at $k = 12$ for both penetration lengths. However, the efficiency is also negative for all cases (not shown).

In order to consider the analogy between the wall-normal and streamwise Lorenz force

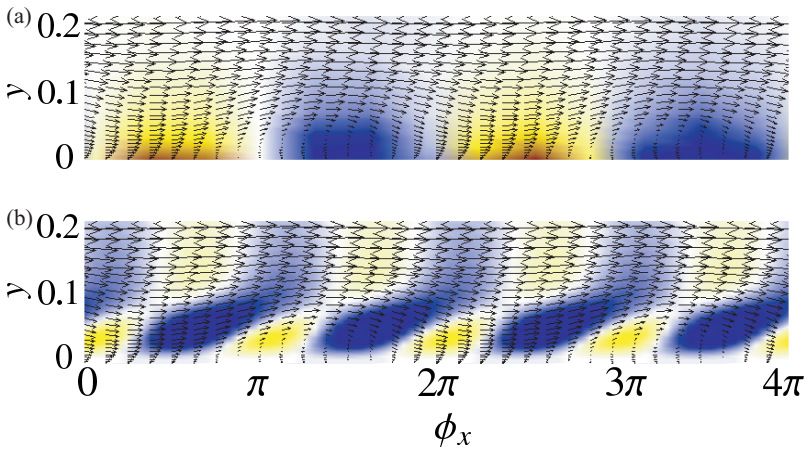

Figure 8. (a) Body force and (b) product of $\widetilde{u}$ and $\widetilde{v}$, with the velocity vector in the laminar flow. The control parameter is set to the same as the reference case.

controls, the transport equation of the spanwise vorticity is considered, i.e.,

$$\frac{\partial \omega_z}{\partial t} + u_j \frac{\partial \omega_z}{\partial x_j} = \omega_j \frac{\partial v_z}{\partial x_j} + \frac{1}{\mathrm{Re}_b} \frac{\partial^2 \omega_z}{\partial x_j \partial x_j} + \underbrace{\left(\frac{\partial F_y}{\partial x} - \frac{\partial F_x}{\partial y} \right)}_{F_{\omega_z}}. \tag{17}$$

The Lorenz force defined in Eqs. (4)-(5) is substituted into the body force term of Eq. (17). For the wall-normal and streamwise Lorenz force controls, this term reads

$$F_{\omega_z} = k^+ \left(-\mathrm{Re}_\tau I \exp\left(-\frac{y^+}{\Delta^+} \right) \sin\left(k \left(x - ct \right) \right) \right), \tag{18}$$

$$F_{\omega_z} = \frac{1}{\Delta^+} \left(-\mathrm{Re}_\tau I \exp\left(-\frac{y^+}{\Delta^+} \right) \cos\left(k \left(x - ct \right) \right) \right), \tag{19}$$

respectively. Namely, the analogy is expected to hold when $k^+ = \frac{1}{\Delta^+}$.

Table 1 shows the parameter set at which this analogy is expected to hold. The drag reduction rate controlled by the wall-normal Lorenz force is found to be larger than that by the streamwise Lorenz force. The net saving rates, however, are less than zero (i.e., no gain) for each cases. Figure 10(a)-(c) shows the flow statistics at this parameter set, i.e., the mean streamwise velocity in the region near the wall, the RSS and the mean velocity gradient, and the RMS (root-mean-square) velocities. While the agreement in the mean velocities is observed as shown in Fig. 10(a), differences can be noticed in the second moments as shown in Fig. 10(b) and (c). The wall-normal Lorenz force appears to suppress velocity flucatuations more than the streamwise Lorenz force. This discrepancy is due to the difference of the energy source: the streamwise Lorenz force supplies the energy into the transport equation of $v'v'$, while the wall-normal Lorenz force does for $u'u'$.

5. Conclusions

Effects of the skin-friction drag reduction controls using the traveling wave-like wall-normal and streamwise Lorenz forces in a fully developed channel flow are investigated by means of the

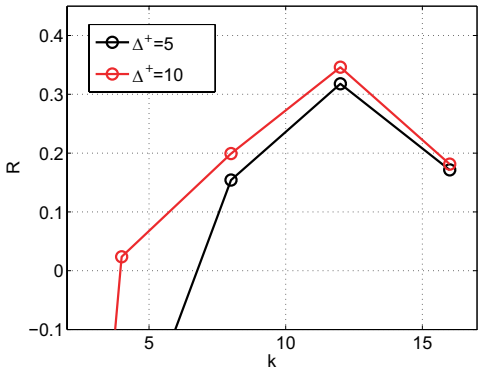

Figure 9. Drag reduction rate as a function of wavespeed controlled by the standing wave-lie streamwise Lorenz force for different wavenumber ($I = 1$, $\Delta^+ = 10$).

Table 1. Input parameters and results at which the analogy is expected to hold.

Body force	I	c	k	Δ^+	R	S
Wall-normal	1	0	8	10	0.34	-0.20
Streamwise	1	0	8	22.5	0.23	-12.0

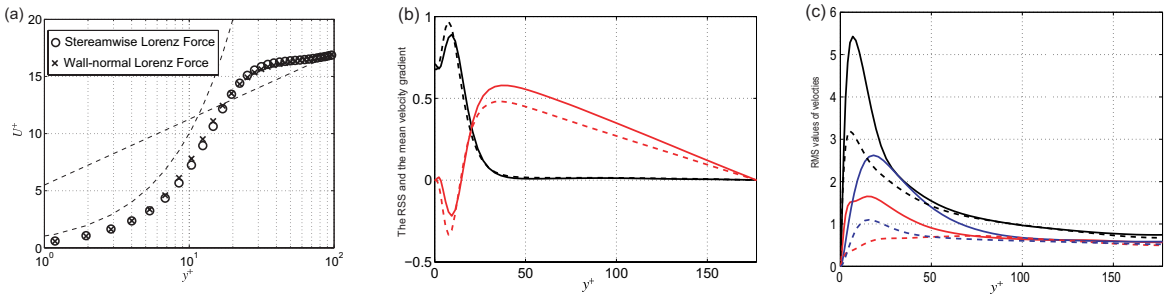

Figure 10. (a) Near-wall velocity. (b) Shear stress balance: black and red lines denote the ordinary RSS, $-\overline{u'v'}$, and the mean velocity gradient, $\partial\overline{u}/\partial y$, respectively, in the wall unit. (c) RMS velocities: black, $u'^+_{\rm rms}$; red, $v'^+_{\rm rms}$; blue, $w'^+_{\rm rms}$. The solid and broken lines denote the streamwise and the wall-normal forcing, respectively, and the parameter set of forcing is shown in Table 1.

direct numerical simulation. It is found that the standing wave can decrease the skin-friction drag, while the positive efficiency is not obtained. For the wall-normal standing wave-like Lorenz force, the negative Reynolds shear stress is generated due to the negative phase component of the Reynolds shear stress. This negative phase-Reynolds shear stress is induced by the spanwise roller-like vortices, which are also observed in the laminar flow. Moreover, the phase relationship of the Fourier coefficient of the velocities in the turbulent flow is found to be similar to that in the laminar flow. While the analogy between the wall-normal and spanwise Lorenz forces is expected, differnces are found in the second moments due to the difference in the energy flow.

Acknowledgments

The authors are grateful to Dr. Shinnosuke Obi (Keio University), Drs. Nobuhide Kasagi and Yosuke Hasegawa (The University of Tokyo), Dr. Kaoru Iwamoto (Tokyo University of Agriculture and Technology). This work was supported through Grant-in-Aid for Scientific Research (A) (No. 20246036) by Japan Society for the Promotion of Science (JSPS), Grant-in-Aid for JSPS Fellows (No. 23·3928), Keio Gijuku Academic Funds, and Global COE program of "Center for Education and Research of Symbiotic, Safe and Secure System Design".

References

Berger, T. W., Kim, J., Lee, C., & Lim, J. 2000 Turbulent boundary layer control utilizing the Lorentz force. *Phys. Fluids* **12**, 631–649.

Bewley, T. R. 2001 Flow control: new challenges for a new Renaissance. *Progress Aero. Sci.* **37**, 21–58.

Belwey, T. R. & Aamo, O. M. 2004 A 'win-winf mechanism for low-drag transients in controlled two-dimensional channel flow and its implications for sustained drag reduction. *J. Fluid Mech.* **499**, 183–194.

Fukagata, K., Iwamoto, K., & Kasagi, N. 2002 Contribution of Reynolds shear stress distribution to the skin friction in wall-bounded flows. *Phys. Fluids* **14**, L73–L76.

Fukagata, K., Kasagi, N., & Koumoutsakos, P. 2006 A theoretical prediction of friction drag reduction in turbulent flow by superhydrophobic surfaces. *Phys. Fluids* **18**, 051703.

Fukagata, K., Kasagi, N., & Sugiyama, K. 2005 Feedback control achieving sublaminar friction drag. *Proc. 6th Symp. on Smart Control of Turbulence, March, Tokyo* , 143–148.

Hussain, A. K. M. F. & Reynolds, W. C. 1970 The mechanics of an organized wave in turbulent shear flow. *J. Fluid Mech.* **41**, 241–258.

Kasagi, N., Suzuki, Y., & Fukagata, K. 2009 Microelectromechanical systems based feedback control of turbulence for skin friction reduction. *Annu. Rev. Fluid Mech.* **41**, 231–251.

Koumoutsakos, P. 1999 Vorticity flux control for a turbulent channel flow. *Phys. Fluids* **11**, 248–250.

Mamori, H., Fukagata, K., & Hoepffner, J. 2010 Phase relationship in laminar channel flow controlled by traveling-wave-like blowing or suction. *Phys. Rev. E* **81**, 046304.

Min, T., Kang, S. M., Speyer, J. L., & Kim, J. 2006 Sustained sub-laminar drag in a fully developed channel flow. *J. Fluid Mech.* **558**, 309–318.

Yakeno, A., Hasegawa, H., & Kasagi, N. 2010 Mechanism of drag reduction by predetermined spatio-temporally periodic control of wall turbulence. *J. Trans/B* **76B**, 555–562.